Dusty Gas Flow past Bodies under Scattering of Rebounded Particles

S. V. Panfilov[a],*, D. A. Romanyuk[a],**, and Yu. M. Tsirkunov[a],***

[a]*Ustinov Baltic State Technical University "VOENMEKh," St. Petersburg, Russia*
*e-mail: panfilov_sv@rambler.ru
**e-mail: romanyuk-da@rambler.ru
***e-mail: yury-tsirkunov@rambler.ru

Abstract—Two-phase gas-particle flow over a flat plate of finite thickness in a channel at a high subsonic velocity and supersonic transverse flow past a cylinder are considered. The leading edge of the plate is wedge-shaped or represents a smooth bluntness of constant radius. The wedge surface and the front bluntness are specified both smooth and rough. The roughness is modeled by a two-dimensional profile based on an experiment. Spherical particles and a mixture of particles in the form of ellipsoids of revolution, rectangular prisms, prisms with flat-cut vertices, and tetrahedrons are considered. The parameters of each of the forms vary. The impact interaction model proposed earlier and consistent with the experimental data on the coefficients of restitution of the center-of-mass velocity is used to determine the translational and rotational velocities of non-spherical particles after rebound. Along with monosized particles, a dispersed phase with a spread of particles in size is considered. The role of the studied factors of random nature which affect the flow pattern and the dispersed phase parameters is found.

In real two-phase flows of a gas with particles, many effects associated with the dispersed phase dynamics are of the random nature, for example, the spread of particles in size, particle-to-particle collisions in the flow, the non-spherical shape of particles, the roughness of surfaces, and turbulent fluctuations in the carrier gas. In the classical theory of two-phase flows of a gas with particles (see, e.g., [1]), all these random effects are neglected.

In two-phase aerodynamics problems when a vehicle moves in an atmosphere that contains fine sand, volcanic ash, or ice particles, the most important factors which determine the flow pattern of the dispersed phase are the scattering of particles in their rebound from the surface of bodies due to their non-spherical shape and surface roughness, as well as the particle size spread [2]. The quartz or synthetic corundum particles used in experiments in wind tunnels also have non-spherical shape and various sizes.

It is relatively easy to take into account the particles spread in size. For this purpose, it is necessary to know the particle size distribution in undisturbed flow. In this case, the log-normal law is most commonly used. In [3–6], flows past bodies were studied taking into account the spread of spherical particles in size. In the present study, the log-normal law is also adopted.

The non-spherical shape of particles affects their aerodynamic characteristics and, especially, the impact interaction with the surface, leading to scattering after rebound. The influence of the non-spherical shape of particles on the force and the moment exerted from the carrier gas is the subject of a number of reviews and recent studies [7–12]. In the last of the cited works, based on direct numerical simulation of flow past non-rotating particles of various irregular shapes with various random orientations in the flow, a detailed study of the drag forces, transverse forces and moments was carried out in the range of moderate Reynolds numbers $\mathrm{Re}_p \in [0, 200]$ ($\mathrm{Re}_p = 2\rho|\mathbf{V} - \mathbf{V}_p|r_p/\mu$ is the Reynolds number in flow about a particle). It was found that the average value of the drag coefficient for particles close to isometric ones, with a small aspect ratio of the largest and smallest sides, the aerodynamic characteristics of particles depends only slightly on their shape and orientation over the entire considered range of the Reynolds

numbers, while the transverse force coefficient and the moment depend more noticeably on the aspect ratio; however, as the Reynolds number increases, the difference decreases. Being rebounded from the surface, the particles can be strongly twisted. The flow about rotating particles is accompanied by appearance of the transverse Magnus force. As shown by preliminary calculations, in the problems considered in the present study the Mach number, the Reynolds number, and the rotational Reynolds number of the carrier gas flow about reflected particles can reach the values $M_p \approx 1.7$, $Re_p \approx 2600$, and $Re_{p\omega} = \rho|\mathbf{\Omega} - \mathbf{\Omega}_p|r_p^2/\mu \approx 1400$, respectively. In these parameter ranges, for intensely rotating particles of non-spherical shape the data on the aerodynamic drag, Magnus force, and damping torque coefficients are not available in the literature. Therefore, in this study these coefficients were calculated as for spherical particles.

In early investigations of the impact interaction of particles with various surfaces, the rebound parameters were experimentally studied depending on the materials of particles and obstacles and the angle of impact. Some empirical relations were proposed for the coefficients of restitution of the normal and tangential velocities of the center of mass of particles in the plane of impact under rebound [13—17]. Relations of this kind were used in modeling the dispersed phase flows in the neighborhood of bodies [18, 19]. At the same time, models of the collision of a particle with an obstacle were developed, including the description of dynamic interaction of a particle with a surface. The model of the sliding impact of a particle is presented in monograph [20]. In the case of the sliding impact, the momentum equation and Coulomb's law of friction with the dynamic friction coefficient were used. This model has been widely used and is now used to calculate the gas-particle flows in channels when the velocity of particle collision with walls is low [21—23]. In [24], the impact velocities typical for aircraft moving in a dusty atmosphere were considered and a three-dimensional model of the rebound of a non-spherical particle from an obstacle was proposed. In this model it was assumed that the tangential velocity of the point of contact of the particle with the surface at the instant of rebound is equal to zero. In [25], this model was extended to the case of nonzero tangential velocity of the point of contact at the instant of rebound. In [26], a semi-empirical model of the impact interaction of a non-spherical particle with a smooth surface was proposed. In this model the sliding of the particle relative to the surface is admitted for the entire time of the impact interaction. It was assumed that the tangential momentum is proportional not only to the normal momentum, as in Coulomb's law, but also to the average tangential velocity of the particle contact point during the impact. The model also took into account orientation of the particle relative to the surface before a collision. On the basis of this model, the average and most probable values of the coefficients of restitution of the normal and tangential velocities of the center of mass of particles of various shapes and a mixture of particles of various shapes with varying shape parameters were determined. The results for average values are in good agreement with the experimental data [15] for the coefficients of restitution of the velocity components of the particle center of mass. It is this model that is used in the present work to study numerically the dispersed phase flow when particles rebound from a surface.

Surface roughness, along with the non-spherical shape of particles, is the most important factor that can lead to significant scattering of reflected particles. Modeling of the surface roughness, especially if it arises as a result of abrasive erosion, is one of the most difficult problems in the aerodynamics of two-phase flows of a gas with particles. In [22], the flow of spherical particles in a channel with rough walls was studied. The roughness profile was not considered and, during the impact interaction of particles with walls, the impact angle was set randomly based on the normal distribution law. Later, in [27], it was proposed to consider the roughness profile by itself, which was described by a quasi-periodic random function. Its parameters were taken so that the scattering indicatrices of reflected particles were close to those obtained for a real, almost two-dimensional roughness profile. As noted in [28], this approach has an important advantage since it allows one to take into account possible multiple collisions of a particle with a rough surface during rebound and also shadow zones at small impact angles. Subsequently, some models of the surfaces with isotropic and anisotropic roughness were proposed [29, 30]. In the present study, a two-dimensional roughness relief is considered. Such a relief is observed in some experiments on the interaction of particles of synthetic corundum and an obstacle of ductile metal in the range of impact velocities of 100—300 m/s. As proposed in [24], the relief is described by a random function.

The aim of this work is to study flow of the dispersed phase taking into account the scattering of non-spherical particles during rebound from a smooth and rough surface and the spread of particles in size with reference to two-phase flow over a plate of finite thickness with various leading edge profiles in a channel with high subsonic velocity and supersonic flow past a cylinder.
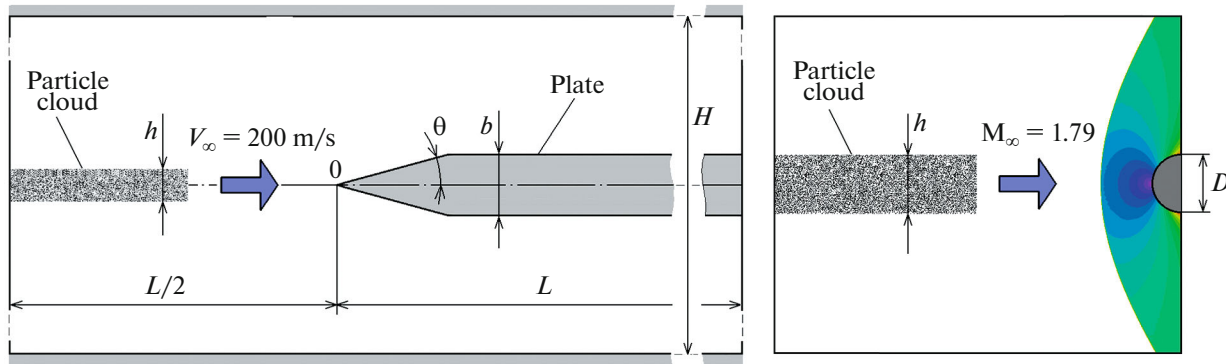
Fig. 1. Diagram of subsonic flow over a plate in a channel (on the left) and supersonic flow past a frontal surface of a cylinder (on the right).

1. FORMULATION OF THE PROBLEM AND THE GAS-PARTICLE FLOW MODEL

1.1. Flow Diagrams

We will consider two problems, namely, symmetrical flow over a flat plate of finite thickness b in a channel of width H and supersonic uniform transverse gas-particle flow in the neighborhood the frontal surface of a cylinder. The plate had the wedge-shaped leading edge, as shown in Fig. 1, or the rounded leading edge with the radius equal to half the plate thickness. The wedge half-angle θ was taken to be equal to $15°$. In an undisturbed flow, the dispersed phase had the appearance of a cloud (Fig. 1). To visualize the features of the dispersed phase flow pattern after rebound of particles, a particle cloud of finite thickness h was considered. In the problem of flow over the plate it was taken $h = b/2$, and in the problem of flow past the cylinder it was taken $h = D$. The cloud length was chosen from the condition of obtaining the stationary particle phase flow patterns. Flow of a mixture of isometric particles of various shapes was studied (Fig. 2), the parameters of each of the shapes were varied as described in [26]. For a plate in a channel, smooth and rough surfaces of a wedge or blunt leading edge were considered; the channel walls were assumed to be smooth. In the problem of transverse flow past a circular cylinder, its surface was assumed to be smooth. To estimate the effect of the spread of particles in size on the particle phase flow pattern, a mixture of monodisperse (identical in mass, although different in shape) and polydisperse particles was studied. The effects associated with the possible destruction of particles and surfaces during impacts were not taken into account.

1.2. Carrier Gas Flow Model

The particle volume fraction was assumed to be very low, so that the effect of particles on carrier gas flow was negligible. In [31] it was shown that such an assumption is valid when the volume particle fraction is less than $\sim 10^{-6}$. In both problems, the characteristic Reynolds numbers are of the order of 10^6. High-inertia particles of synthetic corundum for which the Stokes number was of the order of $10-10^2$ were considered. For such two-phase flow parameters, the boundary layers on the surfaces do not have any effect on particle dynamics, so the gas flow fields were modeled based on the Euler equations. For the compressible gas, in Cartesian coordinates (x, y) the Euler equations take the form:

$$\frac{\partial \mathbf{Q}}{\partial t} + \frac{\partial \mathbf{F}_x}{\partial x} + \frac{\partial \mathbf{F}_y}{\partial y} = 0, \tag{1}$$

where $\mathbf{Q}$ is the vector of conservative variables, and $\mathbf{F}_x$ and $\mathbf{F}_y$ are the vectors of convective terms that are determined by the relations:

$$\mathbf{Q} = \begin{pmatrix} \rho \\ \rho v_x \\ \rho v_y \\ \rho e \end{pmatrix}, \quad \mathbf{F}_x = \begin{pmatrix} \rho v_x \\ \rho v_x^2 + p \\ \rho v_x v_y \\ (\rho e + p)v_x \end{pmatrix}, \quad \mathbf{F}_y = \begin{pmatrix} \rho v_y \\ \rho v_x v_y \\ \rho v_y^2 + p \\ (\rho e + p)v_y \end{pmatrix}, \tag{2}$$

$$p = \rho RT, \quad e = c_V T + (1/2)(v_x^2 + v_y^2). \tag{3}$$

In the above equations, t is time, v_x and v_y are the components of the velocity vector $\mathbf{V}$ along the x and y axes, ρ, p, e and T are the density, the pressure, the specific total energy, and the temperature, respectively, R is the gas constant, and c_V is the specific heat capacity at constant volume.

In the channel flow, the velocity V_∞, the pressure p_∞, and the temperature T_∞ are specified on the inlet boundary, while the pressure p_{out} is specified on the outlet boundary. In the supersonic flow past a cylinder, the velocity, the pressure, and the temperature are also specified on the inlet boundary, while "nonreflecting" conditions are given on the outlet boundary.

1.3. Model of Gas-Particle Interaction

In the present study, collisions between particles are not taken into account and the motion of particles is described based on the Lagrangian approach [20]. The momentum and angular momentum equations for a single particle take the form:

$$m_p \frac{d\mathbf{V}_p}{dt} = \mathbf{f}_p, \quad J_p \frac{d\mathbf{\Omega}_p}{dt} = \mathbf{L}_p, \quad \frac{d\mathbf{r}_p}{dt} = \mathbf{V}_p, \tag{4}$$

where m_p, J_p, $\mathbf{V}_p$, $\mathbf{\Omega}_p$, and $\mathbf{r}_p$ are the mass, the moment of inertia, the velocity, the angular velocity, and the radius-vector of the particle, respectively.

The force $\mathbf{f}_p$ exerted on a particle from the carrier gas includes the drag force $\mathbf{f}_D$ and the transverse Magnus force $\mathbf{f}_M$ ($\mathbf{f}_p = \mathbf{f}_D + \mathbf{f}_M$) which dominate the remaining components of the interphase force in the flows considered. These forces and the moment $\mathbf{L}_p$ exerted on the rotating particle can be expressed in terms of the dimensionless coefficients C_D, C_M, and C_L:

$$\mathbf{f}_D = \frac{1}{2} C_D \pi r_p^2 \rho |\mathbf{V} - \mathbf{V}_p|(\mathbf{V} - \mathbf{V}_p),$$

$$\mathbf{f}_M = \frac{4}{3} C_M \pi r_p^3 \rho [(\mathbf{\Omega} - \mathbf{\Omega}_p) \times (\mathbf{V} - \mathbf{V}_p)],$$

$$\mathbf{L}_p = \frac{1}{2} C_L r_p^5 \rho |\mathbf{\Omega} - \mathbf{\Omega}_p|(\mathbf{\Omega} - \mathbf{\Omega}_p),$$

where $\mathbf{\Omega} = (1/2)\text{curl}\mathbf{V}$

Although we consider non-spherical particles, the model of gas-particle interaction is based on the results for spherical particles. This is partly justified by the closeness of the drag coefficients of non-rotating spherical and non-spherical isometric particles in a wide range of Reynolds numbers in the relative motion (up to $\text{Re}_p \sim 10^3$) [8]. In [32], the drag and lift forces and the moment were numerically studied for non-spherical particles at low Reynolds numbers and relative rotation velocities characteristic of gas-particle flows in pipes. At present, studies of the drag, the lift, and the moment for non-spherical particles in the ranges of flow parameters characteristic of flight conditions in a dusty atmosphere are unknown to the authors. Therefore, in the present study, for the drag, Magnus lift, and moment coefficients we use the relations proposed for spherical particles. These relations approximate the analytical, experimental, and numerical data over a wide range of constitutive parameters in the flow past a particle. Of course, such an approach introduces some error into the model of gas-particle interaction; however, the relations for rapidly rotating non-spherical particles (in the flows considered below, the angular velocity of rotation of particles Ω_p reached $\sim 10^6 - 10^7$ s^{-1}) are not known to the authors.

For the drag coefficient C_D the approximation formulas proposed in [33] were used, in which it was taken $T_p/T = 1$ since C_D in the flows under consideration depends only slightly on the particle/gas temperature ratio:

$$C_D(\text{Re}_p, \text{M}_p) = \begin{cases} C_D^1, & 0 < \text{M}_p \leq 1 \\ C_{D1}^1 + \frac{4}{3}(\text{M}_p - 1)(C_{D2}^2 - C_{D1}^1), & 1 < \text{M}_p \leq 1.75 \\ C_D^2, & \text{M}_p > 1.75, \end{cases}$$

Table 1. The coefficients C_{l1} and C_{l2} for various ranges of the rotational Reynolds number of a particle $\mathrm{Re}_{p\omega}$

$\mathrm{Re}_{p\omega}$	0–6	6–20	20–50	50–4 × 10^4
C_{l1}	0	5.32	6.44	6.45
C_{l2}	16π	37.2	32.2	32.1

$$C_D^1(\mathrm{Re}_p, \mathrm{M}_p) = 24\left\{\mathrm{Re}_p + S\left[4.33 + \frac{2.12}{1.353}\exp\left(-0.247\frac{\mathrm{Re}_p}{S}\right)\right]\right\}^{-1}$$

$$+ \left[\frac{4.5 + 0.38(0.03\,\mathrm{Re}_p + 0.48\sqrt{\mathrm{Re}_p})}{1 + 0.03\,\mathrm{Re}_p + 0.48\sqrt{\mathrm{Re}_p}} + 0.1\mathrm{M}_p^2 + 0.2\mathrm{M}_p^8\right]\exp\left(-\frac{\mathrm{M}_p}{2\sqrt{\mathrm{Re}_p}}\right) + 0.6S\left[1 - \exp\left(-\frac{\mathrm{M}_p}{\mathrm{Re}_p}\right)\right],$$

$$C_D^2(\mathrm{Re}_p, \mathrm{M}_p) = \left[0.9 + \frac{0.34}{\mathrm{M}_p^2} + 1.86\sqrt{\frac{\mathrm{M}_p}{\mathrm{Re}_p}}\left(2 + \frac{1.058}{S} + \frac{2}{S^2} - \frac{1}{S^4}\right)\right]\left(1 + 1.86\sqrt{\frac{\mathrm{M}_p}{\mathrm{Re}_p}}\right)^{-1},$$

$$\mathrm{Re}_p = 2\rho|\mathbf{V} - \mathbf{V}_p|r_p/\mu, \quad \mathrm{M}_p = |\mathbf{V} - \mathbf{V}_p|/\sqrt{\gamma RT}, \quad S = \mathrm{M}_p\sqrt{\gamma/2}.$$

Here, Re_p and M_p are the relative Reynolds and Mach numbers for a particle, C_{D1}^1 is the value of C_D^1 at $\mathrm{M}_p = 1$, and C_{D2}^2 is the value of C_D^2 at $\mathrm{M}_p = 1.75$.

The coefficient C_M was calculated using the exact solution [34] or the approximate formula [35] which depends on the parameter $\gamma_\omega = r_p|\mathbf{\Omega} - \mathbf{\Omega}_p|/|\mathbf{V} - \mathbf{V}_p|$:

$$C_M = \begin{cases} \dfrac{3}{4}, & 2\gamma_\omega < 0.45 \\ \dfrac{3}{8\gamma_\omega}[0.45 + (2\gamma_\omega - 0.45)\exp(-0.075\gamma_\omega^{0.4}\,\mathrm{Re}_p^{0.7})], & 2\gamma_\omega \geq 0.45 \end{cases}$$

The expression for the coefficient C_L was taken in the form proposed in [36]

$$C_L = \frac{C_{l1}}{\sqrt{\mathrm{Re}_{p\omega}}} + \frac{C_{l2}}{\mathrm{Re}_{p\omega}}, \quad \mathrm{Re}_{p\omega} = \frac{\rho|\mathbf{\Omega} - \mathbf{\Omega}_p|r_p^2}{\mu},$$

where $\mathrm{Re}_{p\omega}$ is the rotational Reynolds number and the constants C_{l1} and C_{l2} are given in Table 1.

1.4. Model of Impact Interaction of a Particle and the Surface

The impact interaction of particles with the surface and the particle rebound affect substantially the structure and parameters of gas-particle flow. In two-phase aerodynamics, an important feature of particle-surface collisions is the high collision velocity. Despite the efforts of researchers to develop the impact models that take into account the physical and mechanical properties of particles and the wall [37–39], at present the experimental information on the coefficients of restitution of the velocity components of the centers of mass of particles during rebound is most reliable. In real flows, the particles almost never have the spherical shape. Their orientation at the instant of impact and the direction of rebound are random. Moreover, during reflection a non-spherical particle can hit the wall more than once before it flies into flow. In this study, we use a semi-empirical model of the rebound of non-spherical particles [26], which takes into account the above effects and which is in good agreement with the experimental data [15] on the average values of the coefficients of restitution of the centers of mass of a mixture of particles of various shapes at impact velocities of 50–350 m/s.

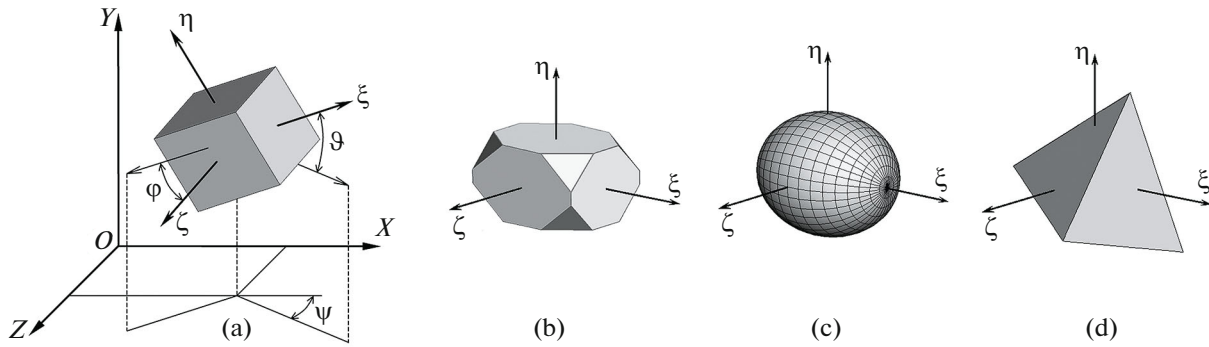The model of rebound includes the description of a single collision of a particle with the rigid surface (Fig. 3).

Fig. 2. Particle shapes and angles φ, ψ, and ϑ, which determine the orientation of a particle in space: rectangular prism (a); prism with flat-cut vertices (b); ellipsoid of revolution (c); tetrahedron (d).
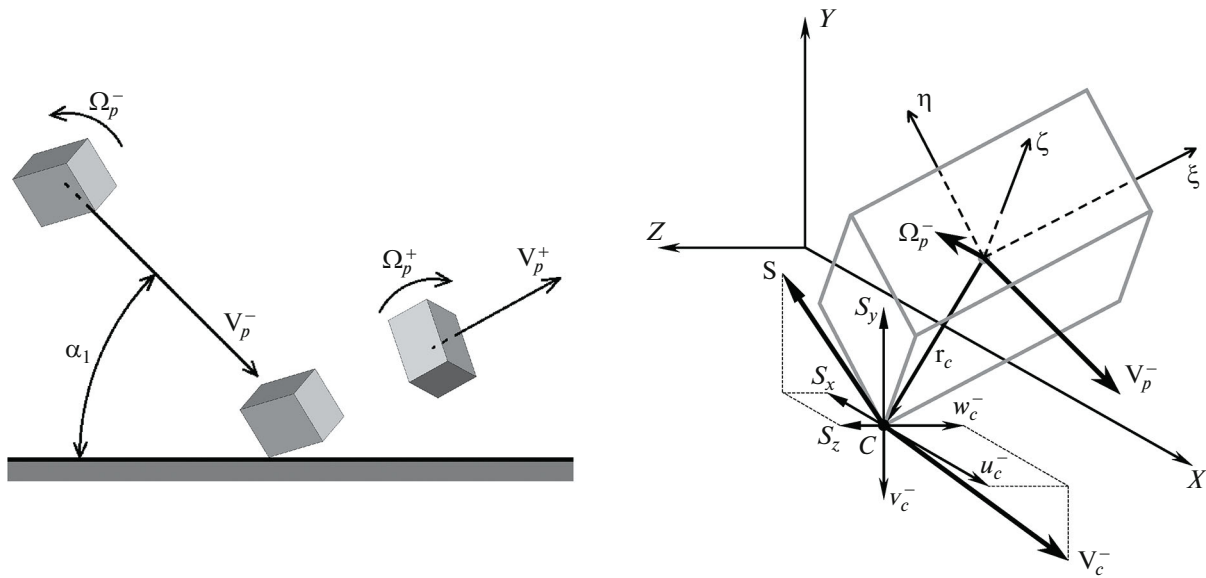

Fig. 3. Collision of a non-spherical particle with a wall.

Assuming that the position of the particle relative to the surface does not vary during a very short time of impact, in integral form the equations for variation in the momentum and the angular momentum of a particle take the form:

$$m_p(\mathbf{V}_p^+ - \mathbf{V}_p^-) \equiv m_p\Delta\mathbf{V}_p = \int_0^{\delta t}\mathbf{f}_c(t)dt \equiv \mathbf{S},$$

$$\|J_p\|(\mathbf{\Omega}_p^+ - \mathbf{\Omega}_p^-) \equiv \|J_p\|\Delta\mathbf{\Omega}_p = \mathbf{r}_c \times \mathbf{S},$$

where m_p and $\|J_p\|$ are the mass and the tensor of inertia of a particle, $\mathbf{f}_c$ and $\mathbf{S}$ are the force and the impulse exerted on the particle at the point of contact, δt is the time interval during which the force $\mathbf{f}_c$ exerts on the particle, the superscripts "−" and "+" denote the particle parameters before and after collision (Fig. 3). A combination of these equations with the kinematic relation

$$\Delta\mathbf{V}_c \equiv \mathbf{V}_c^+ - \mathbf{V}_c^- = \Delta\mathbf{V}_p + \Delta\mathbf{\Omega}_p \times \mathbf{r}_c,$$

which relates the change in the velocity of the point of contact of a particle $\mathbf{V}_c$ with the change in the translational velocity of the particle center of mass $\mathbf{V}_p$ and the angular velocity $\mathbf{\Omega}_p$, gives
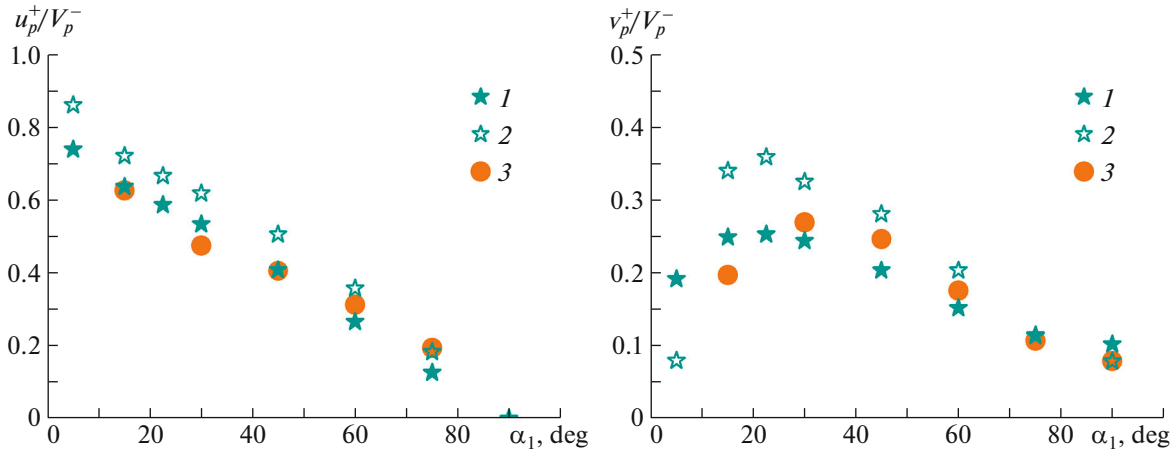
Fig. 4. Average (*1*) and most probable (*2*) values of the relative rebound velocities for a mixture of non-spherical particles of various shapes as functions of the angle of incidence α_1; (*3*) experimental data [15].

$$\frac{1}{m_p}\|J_p\|\Delta\boldsymbol{\Omega}_p = \mathbf{r}_c \times \Delta\mathbf{V}_c - \mathbf{r}_c \times [\Delta\boldsymbol{\Omega}_p \times \mathbf{r}_c].$$

The last equation contains two unknown vectors $\Delta\mathbf{V}_c$ and $\Delta\boldsymbol{\Omega}_p$.

In the case of impact interaction of a rigid non-deformable particle with the wall of an elastic-plastic material at impact velocities typical for the motion of aircraft in a dusty atmosphere, it is assumed that, firstly, the impulse of the force exerted on the particle tangentially to the surface is proportional to both the normal impulse, and the average tangential velocity of the contact point; and secondly, for the coefficient of restitution of the normal component of the particle velocity at the point of contact, the relation can be taken which was obtained experimentally for the normal velocity of the center of mass of the particle by measuring the force exerted on the rigid plate from the dispersed phase.

In this case, for the change in the velocity components of the center of mass of the particle, we can write:

$$\Delta u_p = -C_f(u_c^- + 0.5\Delta u_c)\frac{\Delta v_p}{|\mathbf{V}_c^-|},$$

$$\Delta w_p = -C_f(w_c^- + 0.5\Delta w_c)\frac{\Delta v_p}{|\mathbf{V}_c^-|},$$

$$\Delta v_c = -v_c^-(a_{nc} + 1),$$

where Δu_p, Δv_p, Δw_p and Δu_c, Δv_c, Δw_c are the components of the vectors $\Delta\mathbf{V}_p$ and $\Delta\mathbf{V}_c$ in the coordinate system $OXYZ$ (Fig. 3). The coefficient of dynamic resistance to particle sliding in the tangential direction C_f depends on the mutual position of the vectors $\mathbf{r}_c$ and $\mathbf{V}_p$ ($\mathbf{r}_c$ determines the location of the point of contact with respect to the center of mass of a particle at the instant of impact, Fig. 3). In the present study, for C_f we took the following dependence:

$$C_f = \exp\left[\frac{(\mathbf{r}_c \cdot \mathbf{V}_p^-)}{|\mathbf{r}_c||\mathbf{V}_p^-|}\right].$$

For the parameter a_{nc}, which is the coefficient of restitution of the normal velocity of the particle at the point of contact, we adopt the formula proposed in [15] for a_n:

$$a_{nc} = 1 - [1 - \exp(-0.1|\mathbf{V}_c^-|^{0.61})]\frac{v_c^-}{|\mathbf{V}_c^-|}.$$

Previously, it was established [26] that the average rebound velocities are in the better agreement with the experimental data for a mixture of particles than for particles of a fixed shape. In Fig. 4 we have repro-
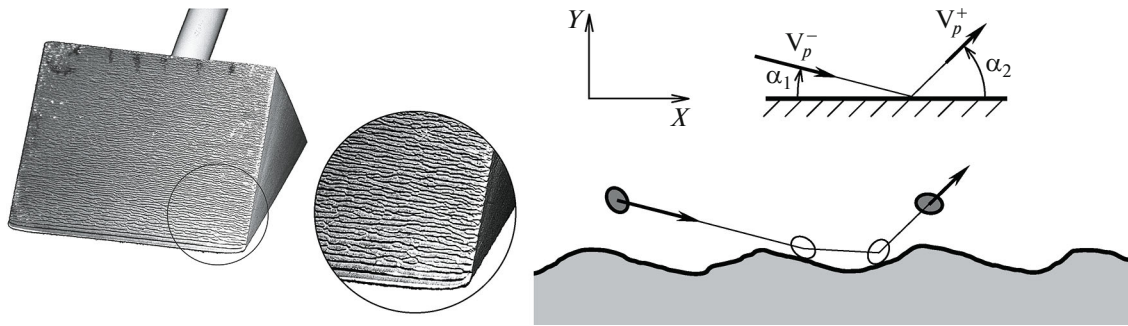
Fig. 5. View of the rough surface of the wedge observed in the experiment (the half-angle of the wedge is equal to 15° and the flow velocity is equal to 200 m/s) and diagram of the rebound of a particle from the rough surface.

duced the results of calculations of the normal and tangential velocity components of the centers of mass for a mixture of particles of various shapes with varying shape parameters in the case of non-rotating incident particles.

1.5. Modeling of Surface Roughness

The surface roughness can significantly affect the particle scattering during rebound and, consequently, the particle phase flow pattern; therefore, the modeling of the roughness relief is important when considering the flow of a gas with solid particles past bodies. One of the reasons for the occurrence of roughness is abrasive erosion of the surface under the action of particle impacts at high velocities (more than 50 m/s). The roughness relief can be both three-dimensional and close to two-dimensional. At present, the authors do not know papers which theoretically describe or numerically simulate the development of roughness during abrasive erosion; however, there are few experimental data on the structure of the surface relief. In the present paper, we consider the roughness relief obtained in experiments on the flow over a wedge of a ductile material in the case of gas flow with particles of synthetic corundum (Fig. 5).

The relief has the form of waves transverse to the direction of flow. In the present study, the roughness profile in the impact plane (X, Y) is modelled by a sine-shaped function $Y(X)$ with random period and amplitude [24]. Given a sequence of N points with random coordinates (X_i, Y_i), where $X_1 = 0$, $X_{i+1} = X_i + h + \xi$, $Y_i = \eta$ ($i = 1, 2, ..., N$), through which a cubic spline is drawn. The quantity $2h$ is the average step of the real roughness profile, random variables ξ and η are taken based on the normal distribution law with mean values equal to zero and standard deviations $\Delta\xi$ and $\Delta\eta$. The quantity $\Delta\eta$ is determined as the average height of the hills. The quantity $\Delta\xi$ is determined from the condition of agreement between the scattering characteristics of reflected particles in the impact plane for the experimental and model roughness profiles. If during the generation of coordinates X_i and Y_i their values were obtained outside the intervals $X_i + h \pm 3\Delta\xi$ and $\pm 3\Delta\eta$, respectively, then this pair of coordinates was eliminated from consideration and the generation was repeated. In the present study, the following values of the profile parameters are taken: $h = 80$ μm, $\Delta\xi = 10$ μm, and $\Delta\eta = 20$ μm.

When modeling the rebound (reflection) of particles from a rough surface, two angles are introduced: the impact angle α_1 shown in Figs. 3 and 5, and the local angle of collision of a particle with a rough surface β_1, which is generally different from α_1. The value of β_1 for each collision is determined by the particle trajectory and the slope of the roughness profile at the collision point. In the case of a smooth surface, obviously, $\beta_1 = \alpha_1$.

Direct numerical simulation of the rebound of a large number of initially non-rotating particles from the smooth and rough surface was performed at various angles of incidence α_1. Spherical particles and a mixture of particles of various shapes were considered. The orientation of non-spherical particles relative to the surface at the instant of the first collision was considered to be random and equiprobable. The possibility of multiple collisions of particles with the surface during the rebound was taken into account. The angle α_1 was varied over the range from 15° to 90° in a step of 15°. Based on the results of calculations of the rebound of 10^8 particles for each value of α_1, the scattering indicatrices of reflected particles in the impact plane were obtained (Fig. 6).
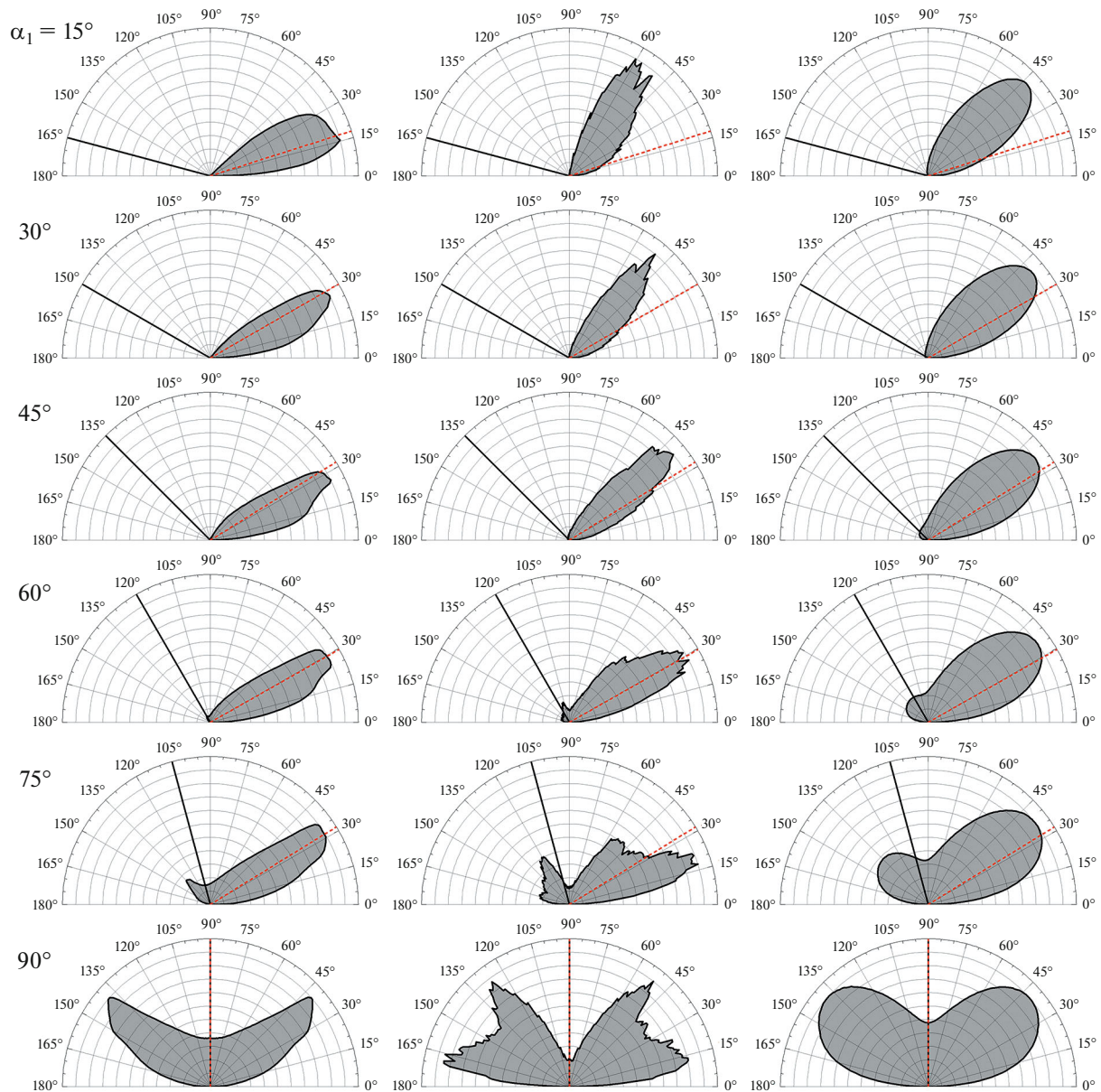
Fig. 6. Scattering indicatrices for reflection of a mixture of non-spherical particles from smooth (on the left) and rough (on the right) surfaces and for reflection of spherical particles from a rough surface (in the center); the direction of rebound of a spherical particle from a smooth surface is shown by a red dashed line.

It can be seen that the surface roughness strongly affects the reflection characteristics of even spherical particles. The scattering indicatrices of non-spherical particles during reflection from the smooth and rough surfaces also differ significantly. Further, when studying the particle phase flow patterns, we will consider both smooth and rough surfaces.

2. RESULTS OF NUMERICAL SIMULATION OF PARTICLE-PHASE FLOW AND THEIR ANALYSIS

This section presents the results of a systematic numerical study of flow patterns of the dispersed phase for flow over a plate of finite thickness in a channel and for supersonic transverse flow past a circular cylinder. In all the cases, air was taken as the carrier gas (the gas constant $R = 287$ J/(kg K) and the heat capacity ratio $\gamma = 1.4$).

Initially, equations (1)-(3) were solved numerically using the CFD method with high accuracy. The total number of grid cells in the channel was 400 thousand. The total number of grid cells in the shock layer near the frontal surface of the cylinder was about 250 thousand. The steady flow was obtained as the steady-state limit reached by the time-dependent solution with time.

To visualize the features of the dispersed phase flow patterns, a cloud was considered (see Fig. 1) in which the particles were located randomly and equiprobably. The Lagrange method was used and equations (4) were numerically solved using the relations for $\mathbf{f}_p$ and $\mathbf{L}_p$ given in Subsection 1.3, as well as the model of impact interaction of a particle with a surface described in Subsection 1.4 was used. For a polydisperse particle phase, the log-normal distribution of particles in size is adopted:

$$g_\infty(d_p) = \frac{1}{\sqrt{2\pi}d_p\ln s}\exp\left[-\left(\frac{\ln d_p - \ln d_g}{\sqrt{2}\ln s}\right)^2\right], \tag{5}$$

where the parameter d_g is related to the most probable particle size d_{pm} by the formula $d_g = d_{pm}\exp(\ln^2 s)$. The calculations were carried out at $s = 1.728$.

2.1. Flow over a Plate in the Channel

The following dimensions of the channel, plate, and particle cloud were taken (Fig. 1): $L = 1$ m, $H = 0.4$ m, $b = 0.02$ m. The inlet boundary was located at the distance $L/2 = 0.5$ m upstream of the leading edge of plate. At the inlet boundary, the velocities of both phases were taken to be identical and equal to $V_\infty = 200$ m/s, the pressure $p_\infty = 100$ kPa, the temperature $T_\infty = 268$ K (the Mach number $\mathrm{M}_\infty = 0.6$ and the Reynolds number $\mathrm{Re}_\infty = \rho_\infty V_\infty H/\mu_\infty \approx 6\times10^6$).

The density of the particle material (corundum) is equal to $\rho_p = 3950$ kg/m³. In the calculations the size (diameter) of spherical and non-spherical monodisperse particles d_p was equal to 32 μm (characteristic Stokes number $\mathrm{Stk} = \rho_p^\circ d_p^2 V_\infty/(18\mu_\infty b) \approx 4$). For the polydisperse particles the size was varied in the calculations within approximately from 4 to 200 μm.

A plate with a smooth and rough wedge-shaped and rounded leading edge was considered.

In Fig. 7 we have reproduced the instantaneous patterns of particles from the initial cloud (see Fig. 1) when the flow takes place over a plate with a wedge-shaped leading edge at an angle $\theta = 15°$. In Fig. 8 we have reproduced similar particle patterns near a plate with the rounded leading edge. The number of visualizing particles in each of the figures was chosen so as to represent most expressively the features of the flow of the dispersed phase. The flow pattern over the plate of monodisperse spherical particles after their rebound from the round leading edge with the rough surface (Fig. 8b) qualitatively differs from other patterns. At first glance, this seems unexpected. In this case, an analysis of the behavior of particles shows that the pronounced "splitting" of the layer of particles with an increased concentration in the case of a rounded leading edge is associated with the appearance of two dominant directions of rebound of spherical particles from the rough surface at angles of incidence close to $\alpha_1 = 90°$ (Fig. 6). A similar situation also occurs in the case of non-spherical particles, but the irregularity of their rebound leads to an additional scattering. This smooths the "splitting" of the layer of particles with a higher concentration.

During the motion of a polydisperse mixture of non-spherical particles, the Mach number M_p reached 0.9 immediately after particle rebound for a wedge-shaped leading edge and up to 1.25 for a rounded leading edge. Further downstream, the Mach number monotonically decreased until rebound from the channel walls, when it reached values in the range from 0.2 to 0.5, and then monotonically decreased again. The Reynolds number Re_p varied in a similar way. At the instant of the first rebound, Re_p reached 1600–2700 and then decreased until the next rebound from the channel walls. The highest value of the rotational Reynolds number Re_ω reached 500–1200. The smaller value corresponds to the blunted leading edge of the plate, and the largest one corresponds to the wedge-shaped edge.

Along with the study of the flow patterns of particles from the initially thin near-axial homogeneous cloud, the flow of the entire dispersed phase in the channel was also studied, including those particles which did not collide with the plate and the channel walls. In Fig. 9 we have reproduced two examples of the complete flow patterns of a monodisperse phase in the case of flow over a plate with the round leading edge and the corresponding relative particle concentration profiles $\overline{\phi}_p = \phi_p/\phi_{p\infty}$ ($\phi_{p\infty}$ is the volume particle concentration in the undisturbed flow) in the outlet channel cross-section. In these flow fields, two layers with an increased particle concentration are formed. One layer consists of reflected particles, the
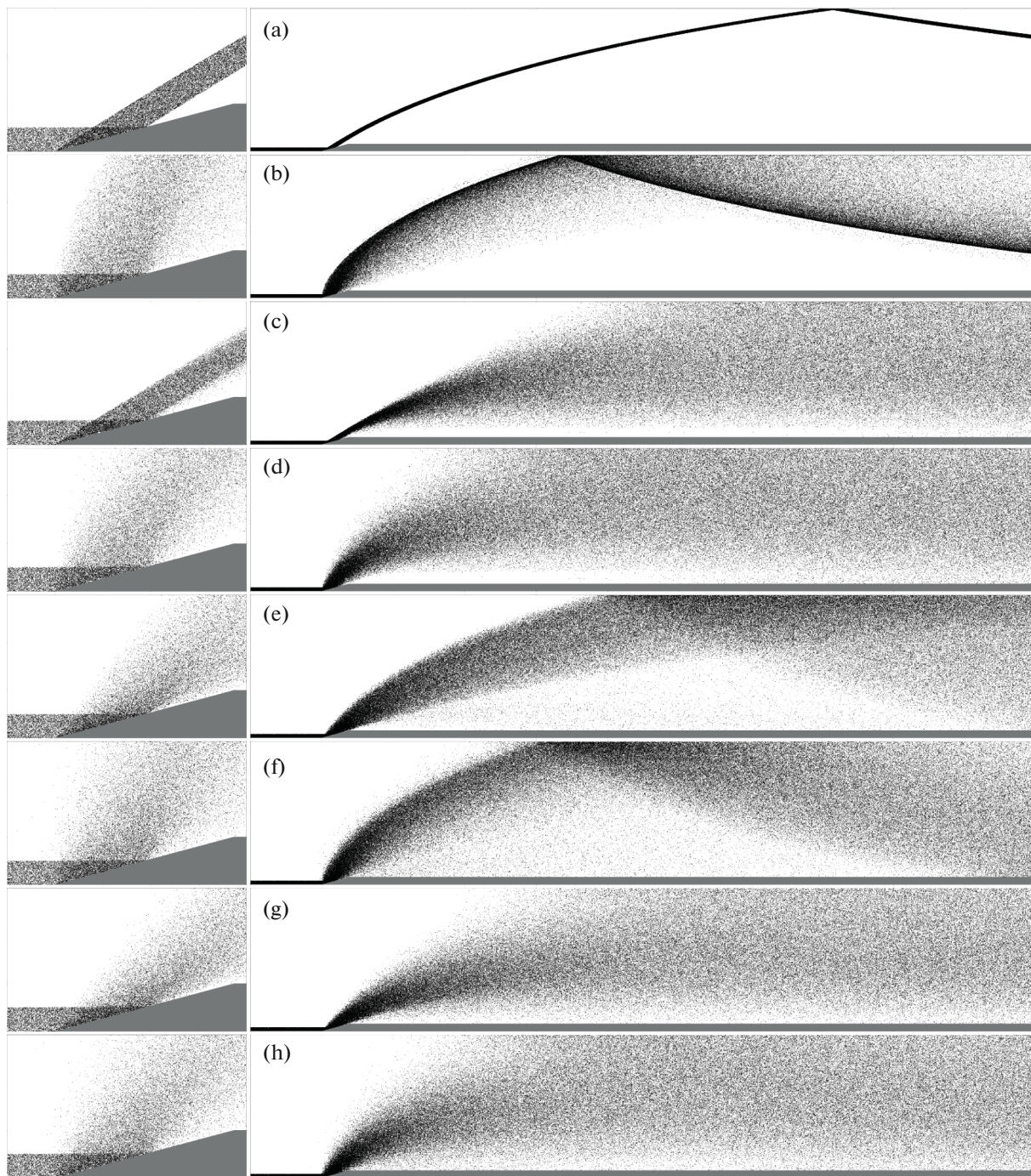
Fig. 7. Particle cloud flow patterns near the leading edge of the plate (on the left, enlarged) and downstream in the channel (on the right): $\theta = 15°$; (a)–(d) correspond to spherical particles; (e−h) correspond to a mixture of non-spherical particles; (a, b, e, f) correspond to monodisperse particles; (c, d, g, h) correspond to polydisperse particles; (a, c, e, g) correspond to the smooth surface of the wedge; and (b, d, f, h) correspond to the rough surface of the wedge.

other appears near the plate on the boundary of the particle-free region and consists of particles that had no collisions with the plate. The profiles of the relative volume particle concentration were also calculated for all considered cases of the dispersed phase and the surface of the leading edge. The main results are shown in Fig. 10. It can be seen that in the case of spherical monodisperse particles, two maxima are always obtained, both for the wedge-shaped and for the blunt leading edge of the plate. For a monodisperse mixture of nonspherical particles, only one maximum appears on the boundary of the particle-
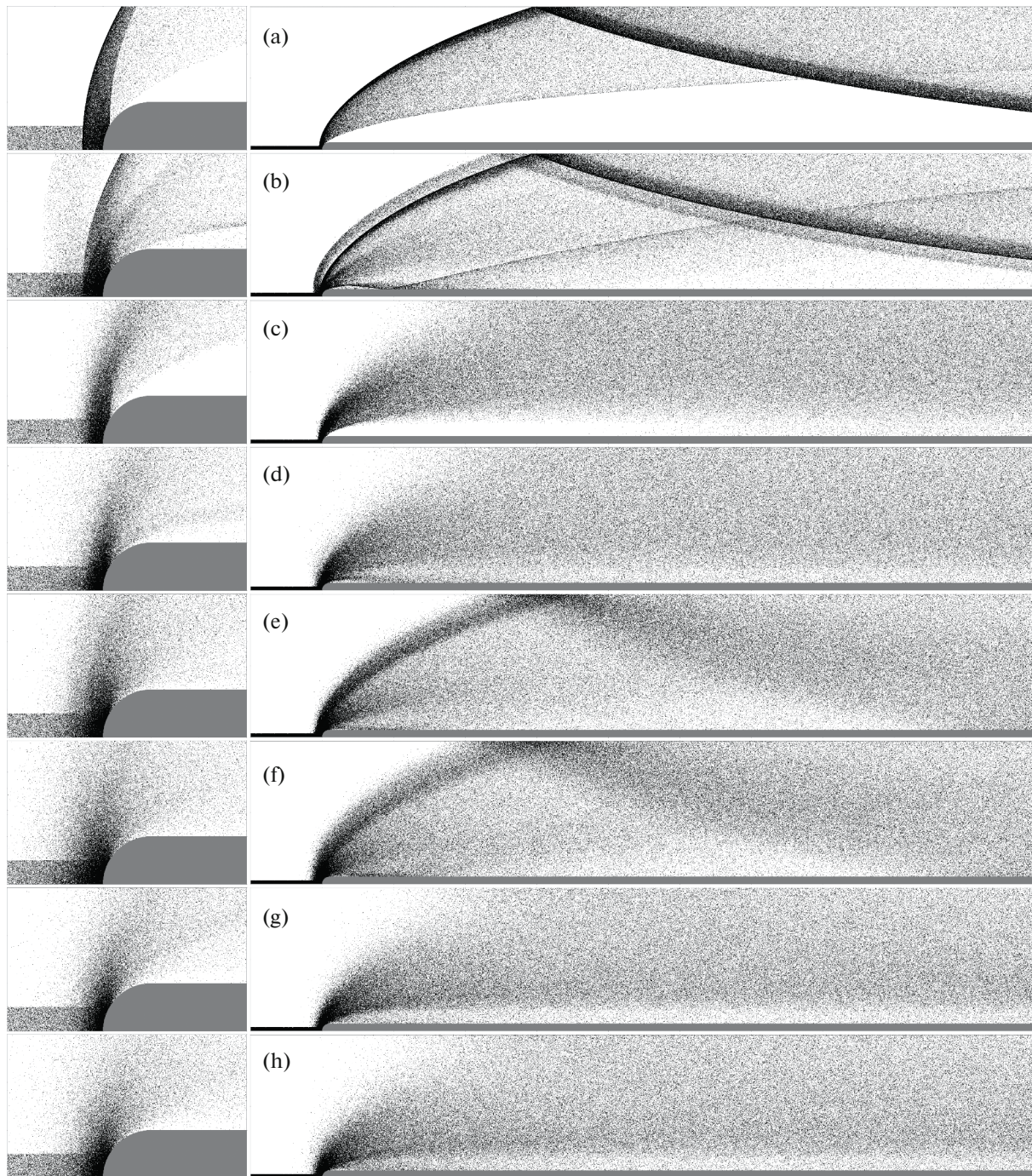
Fig. 8. Particle cloud flow patterns near the rounded leading edge of the plate (on the left, enlarged) and downstream in the channel (on the right): (a−d) correspond to spherical particles; (e−h) correspond to a mixture of non-spherical particles; (a, b, e, f) correspond to monodisperse particles; (c, d, g, h) correspond to polydisperse particles; (a, c, e, g) correspond to the smooth surface of the rounded edge; and (b, d, f, h) correspond to the rough surface of the rounded edge.

free region. In the case of the blunt leading edge, this maximum is very sharp, regardless of whether the spherical particles or the mixture of non-spherical particles are considered and whether the blunt surface is smooth or rough. The relative volume concentration of particles in this maximum reaches $\overline{\phi}_p \approx 5.4$. From the classification of singularities in the collisionless medium of particles, this maximum corresponds to a caustic. As can be seen from Fig. 10, for the taken parameters of the two-phase flow, the
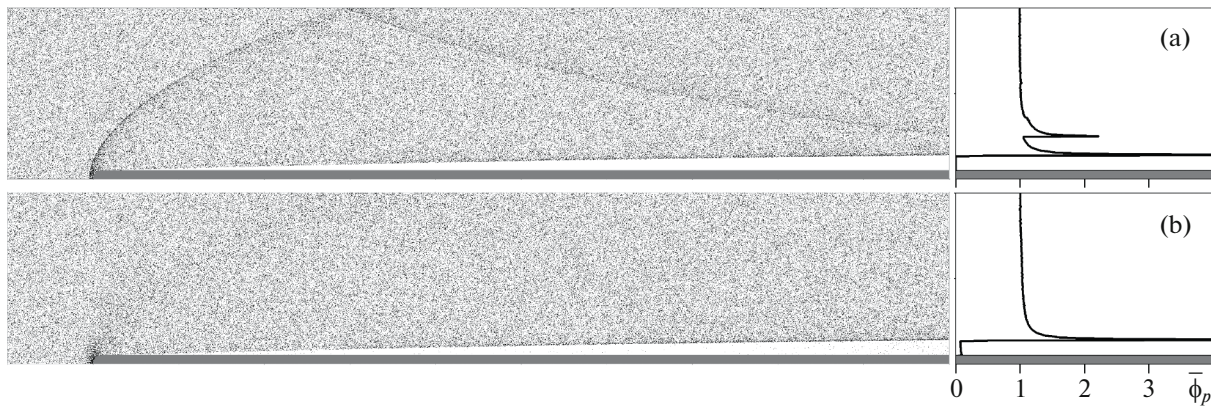
Fig. 9. Full patterns of monodisperse particles flow in a channel near a plate with the rounded leading edge (on the left) and profiles of the relative particle volume fraction $\overline{\phi}_p$ in the outlet section of the channel (on the right): spherical particles, smooth blunt surface (a); and a mixture of non-spherical particles, rough blunt surface (b).
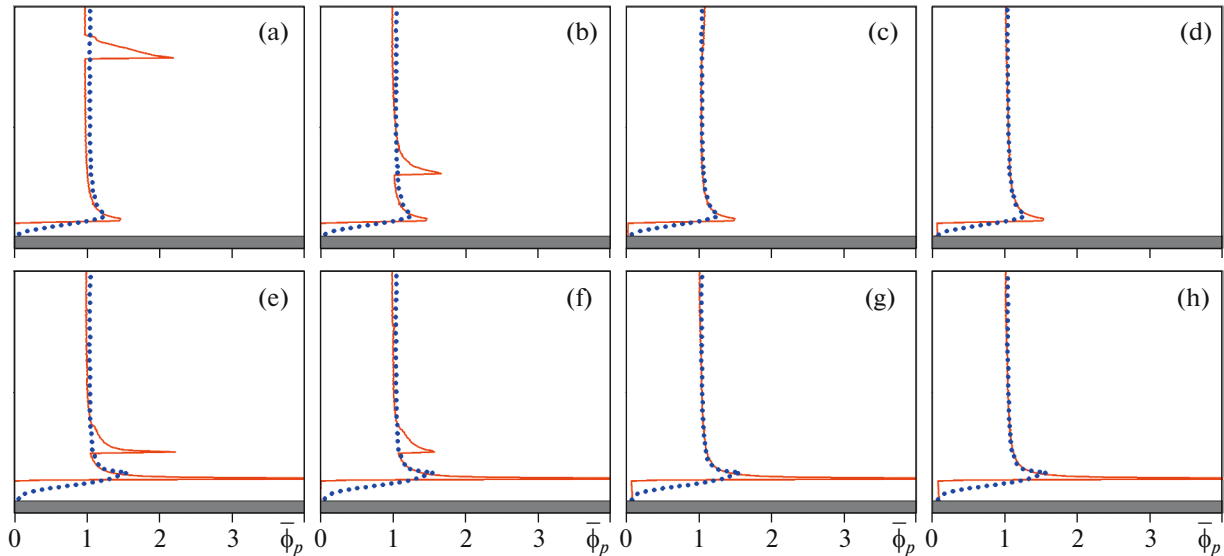

Fig. 10. Profiles of the relative particle volume fraction $\overline{\phi}_p$ in the outlet section of the channel in the flow past a plate with the wedge-shaped leading edge (top row) and with a rounded leading edge (bottom row): solid curves correspond to the monodisperse particles, dots to the polydisperse particles; (a, b, e, f) correspond to spherical particles; (c, d, g, h) correspond to a mixture of non-spherical particles; (a, c, e, g) correspond to smooth and (b, d, f, h) to rough surface of wedge or blunt.

polydispersity of particle phase has the greatest effect on the concentration profiles. Different fractions are mixed in the disturbed flow region and, as a result, the concentration profiles are smoothed out and the maximum decreases significantly.

2.2. Supersonic Flow past a Cylinder

In numerical simulation, the following input data were taken: the cylinder diameter $D = 20$ mm, the free-stream flow velocity $V_\infty = 300$ m/s, the pressure $p_\infty = 50$ kPa, and the temperature $T_\infty = 70$ K. The particles represent sand (the density of 2650 kg/m³), the size of monodisperse particles and the most probable size of polydisperse particles d_p are equal to 4 and 10 μm. These values correspond to the Mach and Reynolds numbers $M_\infty = 1.79$ and $Re_\infty = \rho_\infty V_\infty D / \mu_\infty \approx 3 \times 10^6$ and the characteristic Stokes number $Stk = \rho_p^\circ d_p^2 V_\infty / (18 \mu_\infty D) \approx 1.8$–11.
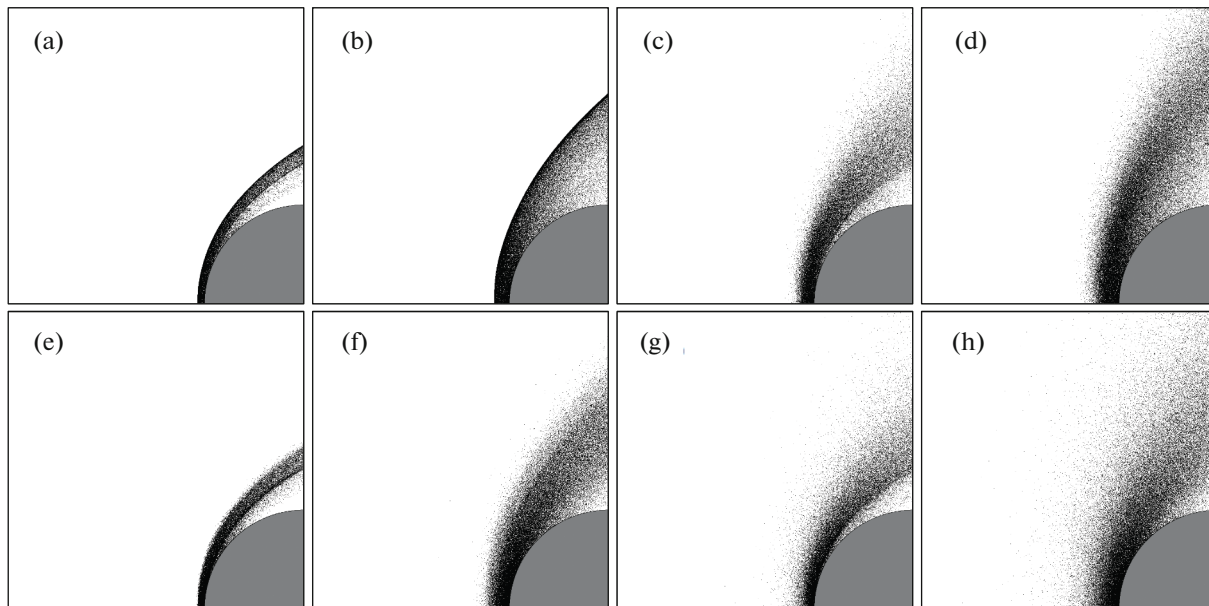
Fig. 11. The flow pattern of reflected particles in the shock layer near the frontal surface of the cylinder: spherical particles at the top, a mixture of non-spherical particles at the bottom; (a, b, e, f) correspond to monodisperse particles, (c, d, g, h) correspond to polydisperse particles; (a, c, e, g) correspond to the size d_p or the most probable size d_{pm} is equal to 4 μm, and (b, d, f, h) correspond to the size or the most probable size of 10 μm.

The influence of scattering of non-spherical particles upon rebound from the surface and the effect of particles spread in size on the flow structure of the dispersed phase were studied. The interaction of a cloud of particles with the cylinder was simulated (see Fig. 1). The cylinder surface was assumed to be smooth. The results are given in Fig. 11.

As can be seen, the smaller particles ($d_p = 4$ μm) scatter more weakly and relax faster towards the carrier gas flow. The larger particles ($d_p = 10$ μm) bounce over a greater distance, scatter more strongly, and form a much thicker layer of reflected particles. The polydispersity of the particle phase leads to mixing of the fractions even when the particles move towards the cylinder in the shock layer. Subsequently, the spread of particles in size leads to a significant "smearing" of the layer of reflected particles.

One of the most negative phenomena when a body moves in a dusty atmosphere is abrasive erosion of its surface. As a result of multiple particle impacts, a rough surface relief appears and further destruction of the body with mass loss can occur. The erosion process depends on the physico-mechanical properties of the particles and the body and on the velocity and the angle of impact [40]. The effect of the dispersed phase on the body can be estimated from losses of the kinetic energy of particles during rebound. In the general case, the kinetic energy losses are distributed between the reflected particles and the body and include heating, deformation and destruction. If the particles are not deformed and are not destroyed in the impacts, and the material of body is elastic-plastic, then the energy losses of the particles are distributed between heating, deformation and destruction of the body. On the basis of calculations of a large number ($\sim 10^6$) of collisions of particles with the surface of cylinder, the dependences of the relative loss of the kinetic energy of particles upon reflection were found. The results obtained are presented in Fig. 12 (E is the kinetic energy flux of incident particles and ΔE is the losses of the kinetic energy during reflection).

The symbols correspond to the average values of particle energy losses during rebound from the surface of a cylinder in the ranges of the angle φ from 0° to 10°, from 10° to 20°, etc. The maximum energy losses (the maximum intensity of the total - thermal and erosive − action of the particle phase on the cylinder) are observed near the forward point $0° \leq \varphi \leq 10°$ and with increase in φ (with decrease in the impact angle α_1, Fig. 3), they decrease, in the case of a monodisperse particles to zero in the region $80° \leq \varphi \leq 90°$. The latter is explained by the absence of collisions of particles with the surface here, since a region free from particles appears near the midsection (see Fig. 11). Note that for ductile materials, the most intense destruction occurs at the impact angles $\alpha_1 \sim 20°$ [40]. This allows us to conclude that the particle energy
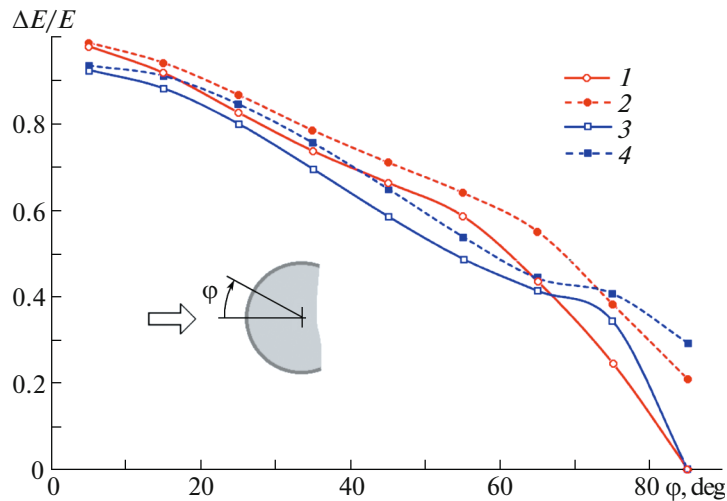
Fig. 12. Relative losses of the kinetic energy of a dispersed particles during their impact interaction with the cylinder surface: the size of monodisperse particles or the most probable size of polydisperse particles $d_p = d_{pm} = 10$ μm; curves *1* and *2* correspond to the spherical particles, curves *3* and *4* correspond to a mixture of particles of various shapes; curves *1* and *3* correspond to the monodisperse particles, and curves *2* and *4* to the polydisperse particles.

losses in a wide vicinity of the forward point are mainly distributed between heating and plastic deformation.

SUMMARY

The numerical simulation of two-phase flow of gas with particles at a high subsonic velocity near the plate of finite thickness in a channel and at a supersonic velocity near a cylinder was performed. The main attention was paid to random effects: the scattering of particles reflected from the surfaces due to their non-spherical shape and surface roughness, as well as the spread of particles in size. A mixture of non-spherical particles of several shapes was considered, namely, ellipsoids, rectangular prismatic particles, prisms with flat-cut vertices, and tetrahedrons. The parameters of the shapes were varied. A new model of impact interaction was used to calculate the translational and rotational velocities of particles after rebounding from the surface. This model ensures good agreement with experimental data on the average values of the coefficients of restitution of the normal and tangential velocities over the entire range of impact angles. Inertial particles were considered (the characteristic Stokes number Stk: Stk $\approx 1.8-11$). The results were compared with those obtained for spherical particles.

The study showed that the scattering of particles during reflection and their polydispersity radically change the particle phase flow pattern, and these effects should be taken into account when simulating gas flows with particles in problems of two-phase aerodynamics.

The reflection of particles is accompanied by the loss of their kinetic energy. Such losses are associated with heating and abrasive surface erosion. The erosion process leads to a change in the surface topography and subsequent mass removal. At present, there are no models that describe the process of formation of a surface roughness relief as a result of erosion, and here the results of experiments are the most reliable. The appearance of surface roughness affects not only the scattering of particles during rebound, as shown in this study, but can affect friction, heat flux, and laminar-turbulent transition in the boundary layer, and it is important to take into account in aerodynamic problems.

FUNDING

OPEN ACCESS

REFERENCES

1. Nigmatulin, R.I., *Dynamics of Multiphase Media,* vol. 1, New York: Hemisphere, 1990; Moscow: Nauka, 1987.

2. Tsirkunov, Yu.M., Panfilov, S.V., and Romanyuk, D.A., Two-phase gas flows with particles in aerodynamic problems: the view of a scientist and an engineer, problems and results, in: *IX Polyakhov's Readings: Proceedings of the International Scientific Conference on Mechanics, March 9−12, 2021, St. Petersburg, Russia,* St. Petersburg: VVM Publishing House, 2021, pp. 63−67.

3. Tsirkunov, Yu.M., Study of inertial settling of polydisperse particles at the stagnation point of a sphere, *Zh. Prikl. Mekh. Tekh. Fiz.,* 1985, no 5, pp. 94−102.

4. Molleson, G.V. and Stasenko, A.L., Peculiarities of flow over a blunted body by a supersonic polydispersed jet with a swirl of reflected particles, *High Temperature*, 2011, vol. 49, no. 1, pp. 72−80.

5. Tsirkunov, Yu., Romanyuk, D., and Panfilov, S., Effects of particle mixing and scattering in the dusty gas flow through moving and stationary cascades of airfoils, in: *Progress in Propulsion Physics*, vol. 2, Ed. by L. DeLuca, C. Bonnal, O. Haidn, and S. Frolov, Torus Press and EDP Sciences, 2011, pp. 459−474.

6. Reviznikov, D.L., Sposobin, A.V., and Sukharev,T.Yu., Numerical simulation of the flow around a blunt body in supersonic polydisperse stream, *High Temperature*, 2017, vol. 55, no. 3, pp. 400−406.

7. Haider, A. and Levenspiel, O., Drag coefficient and thermal velocity of spherical and nonspherical particles, *Powder Technology*, 1989, vol. 58, pp. 63−70.

8. Hölzer, A. and Sommerfeld, M., New simple correlation formula for the drag coefficient of non-spherical particles, *Powder Technology*, 2008, vol. 184, pp. 361−365.

9. Kashevarov, A.V. and Stasenko, A.L., Interaction of particles of various shapes with a carrier continuum gas flow (review), *Uch. Zap. TsAGI*, 2014, vol. 45, no. 5, pp. 3−17.

10. Sommerfeld, M. and Qadir, Z., Fluid dynamic forces acting on irregular shaped particles: simulations by the Lattice−Boltzmann method, *Int. J. Multiphase Flow*, 2018, vol. 101, pp. 212−222.

11. Sanjeevi, S.K.P., Kuipers, H.A.M., and Padding, J.T., Drag, lift and torque correlations for non-spherical particles from Stokes limit to high Reynolds numbers, *Int. J. Multiphase Flow*, 2018, vol. 106, pp. 325−337.

12. Castang, C., Laín S., García, D., and Sommerfeld, M., Aerodynamic coefficients of irregular non-spherical particles at intermediate Reynolds numbers, *Powder Technology*, 2022, vol. 402, p. 117341.

13. Grant, G. and Tabakoff, W. Erosion prediction in turbomachinery resulting from environmental solid particles, *J. Aircraft.*, 1975, vol. 12, pp. 471−478.

14. Tabakoff, W., Malak, M.F., and Hamed, A., Laser measurements of solid-particle rebound parameters impacting on 2024 aluminium and 6A1-4V titanium alloys, *AIAA J.*, 1987, vol. 25, no. 5, pp. 721−726.

15. Lashkov, V.A., Experimental determination of the coefficients of restitution of particles in the flow of a gas suspension in a collision against the surface, *J. Eng. Phys. Thermophys*, 1991, vol. 60, no. 2, pp. 154−159.

16. Tabakoff, W., Measurements of particles rebound characteristics on materials used in gas turbines, *J. Propulsion,* 1991, vol. 7, no. 5, pp. 805−813.

17. Tsirkunov, Yu.M., Panfilov, S.V., and Klychnikov, M.B., Semiempirical model of impact interaction of a disperse impurity particle with a surface in a gas suspension flow, *J. Engng. Phys. Thermophys.*, 1994, vol. 67, nos. 5−6, pp. 1018−1025.

18. Vittal, B.V.R. and Tabakoff, W., Two-phase flow around a two-dimensional cylinder, *AIAA J.*, 1987, vol. 25, no. 5, pp. 648−654.

19. Volkov, A.N. and Tsirkunov, Yu.M., Kinetic model of a collisional admixture in dusty gas and its application to calculating flow past bodies, *Fluid Dyn.*, 2000, vol. 35, no. 3, pp. 380−392. https://doi.org/10.1007/BF02697751

20. Crowe, C.T., Schwarzkopf, J.D., Sommerfeld, M., and Tsuji, Y., *Multiphase Flows with Droplets and Particles*, 2nd ed., Boca Raton: CRC Press, 2012.

21. Tsuji Y., Oshima, T., and Morikawa, Y., Numerical simulation of pneumatic conveying in a horizontal pipe, *KONA Powder Part. J.*, 1985, no. 3, pp. 38−51.

22. Sommerfeld, M., Modelling of particle-wall collisions in confined gas-particle flows, *Int. J. of Multiphase Flow,* 1992, vol. 18, no. 6, pp. 905−926.

23. Sommerfeld, M. and Huber, N., Experimental analysis and modelling of particle-wall collisions, *Int. J. Multiphase Flow*, 1999, vol. 25, pp. 1457−1489.

24. Panfilov, S.V. and Tsirkunov, Yu.M., Scattering of non-spherical particles rebounding from a smooth and a rough surface in a high-speed gas−particle flow, *J. Appl. Mech. Tech. Phys.*, 2008, vol. 49, no. 2, pp. 222−230.

25. Quintero, B., Lain, S., and Sommerfeld, M., Derivation and validation of a hard-body particle-wall collision model for non-spherical particles of arbitrary shape, *Powder Technology*, 2021, vol. 380, pp. 526−538.

26. Panfilov, S.V. and Tsirkunov, Yu.M., Model of non-spherical particles' rebound and scattering at high speed interaction with a streamlined surface, *Tech. Phys.,* 2022, vol. 92, no. 5, pp. 570−581. https://doi.org/10.21883/TP.2022.05.53671.324-21

27. Tsirkunov, Yu.M. and Panfilov, S.V., Modelling of particle-wall interaction in two-phase flows at moderate and high particle impact velocity, in: *Proc. of the Third Int. Conf. on Multiphase Flow*, ICMF'98, Lyon, France, June 8−12, 1998, Paper 693.

28. Konan, N.A., Kannengieser, O., and Simonin, O., Stochastic modeling of the multiple rebound effects for particle-rough wall collisions, *Int. J. Multiphase Flow*, 2009, vol. 35, pp. 933−945.

29. Radenkovic, D. and Simonin, O., Stochastic modelling of three-dimensional particle rebound from isotropic rough wall surface, *Int. J. Multiphase Flow*, 2018, vol. 109, pp. 35−50.

30. Radenkovic, D. and Simonin, O., Modelling of three-dimensional particle rebound from an anisotropic rough wall, *Powder Technology*, 2021, vol. 393, pp. 165−183.

31. Tsirkunov, Yu.M., Gas-particle flows around bodies − key problems, modeling and numerical analysis, in: *Proc. 4th Int. Conf. on Multiphase Flow: CD-ROM Proceedings ICMF'2001, May 27−June 1, 2001, New Orleans, LA, USA,* Ed. by E. Michaelides, Paper no. 607, pp. 1−31, 2001.

32. Hőlzer, A. and Sommerfeld, M., Lattice Boltzmann simulations to determine drag, lift and torque acting on non-spherical particles, *Computers and Fluids*, 2009, vol. 38, pp. 572−589.

33. Henderson, Ch.B., Drag coefficients of spheres in continuum and rarefied flows, *AIAA J.*, 1976, vol. 14, no. 6, pp. 707−708.

34. Rubinow, S.I. and Keller, J.B., The transverse force on a spinning sphere moving in a viscous fluid, *J. Fluid Mech.*, 1961, vol. 11, pp. 447−459.

35. Oesterlé, B. and Bui Dinh, T., Experiments on the lift of a spinning sphere in a range of intermediate Reynolds numbers, *Experim. in Fluids,* 1998, vol. 25, pp. 16−22.

36. Dennis, S.C.R., Singh, S.N., and Ingham, D.B., The steady flow due to a rotating sphere at low and moderate Reynolds numbers, *J. Fluid Mech.*, 1980, vol. 101, pp. 257−279.

37. Stasenko, A.L., Velocity recovery factors of a particle repelled from a solid surface, *J. Eng. Phys. Thermophys*, 2007, vol. 80, no. 5, pp. 885−891.

38. Lashkov, V.A., Coefficient of restitution of the velocity for direct impact, *Vestnik of St. Petersburg State University*, S*er.* 1, 2010, no. 4, pp. 127−136.

39. Ray, S., Kempe, T., and Frölich, J., Efficient modelling of particle collisions using a nonlinear viscoelastic contact force, *Int. J. Multiphase Flow,* 2015, vol. 76, pp. 101−110.

40. *Erosion,* Ed. by Preece, C., New York: Academic, 1979.

Translated by E.A. Pushkar